Chapter 2

Thermal Stability of the Nanostructured Powder Mixtures Prepared by Mechanical Alloying

Safia Alleg, Saida Souilah and Joan Joseph Suñol

Additional information is available at the end of the chapter

http://dx.doi.org/10.5772/54151

1. Introduction

Nanocrystalline materials present an attractive potential for technological applications and provide an excellent opportunity to study the nature of solid interfaces and to extend knowledge of the structure-property relationship in solid materials down to the nanometer regime. Nanocrystalline materials can be produced by various methods such as mechanical alloying, inert gas condensation, sol–gel process, electrodeposition, chemical vapour deposition, heat treatment of amorphous ribbons, high speed deformation, etc. Mechanical alloying is a non-equilibrium process resulting in solid state alloying beyond the equilibrium solubility limit. During the milling process, mixtures of elemental or prealloyed powders are subjected to heavy plastic deformation through high-energy collision from the balls. The processes of fracturing and cold welding, as well as their kinetics and predominance at any stage, depend mostly on the deformation characteristics of the starting powders. As a result of the induced heavy plastic deformation into the powder particles during the milling process, nanostructured materials are produced by the structural decomposition of coarser-grained structure. This leads to a continuous refinement of the internal structure of the powder particles to nanometer scales.

Solid-state processing is a way to obtain alloys in states far-from-equilibrium. The microstructural manifestations of the departures from equilibrium achieved by mechanical alloying can be classified as follows: (i) **augmented defect concentrations** such as vacancies, interstitials, dislocations, stacking faults, twin boundaries, grain boundaries as well as an increased level of chemical disorder in ordered solid solutions and compounds; (ii) **microstructural refinement** which involves finer scale distributions of different phases and of solutes; (iii) **extended solid solubility**; a stable crystalline phase may be found with solute levels beyond the solubility limit at ambient temperature, or beyond the equilibrium limit at any temperature; and (iv) **metastable phases** which may form during processing like crystalline, quasicrystalline and intermetallic compounds. Chemical reactions can

proceed towards equilibrium in stages, and the intermediate stages can yield a metastable phase. In the solid state amorphization reaction, an amorphous alloy can be produced by the reaction of two solid metallic elements. Severe mechanical deformation can lead to metastable states. The deformation forces the production of disturbed configurations or brings different phases into intimate contact promoting solid-state reactions.

The alloying process can be carried out using different apparatus such as planetary mills, attrition mills, vibratory mills, shaker mills, etc. [1]. A broad range of alloys, solid solutions, intermetallics and composites have been prepared in the nanocrystalline, quasicrystalline or amorphous state [2-10]. A significant increase in solubility limit has been reported in many mechanically alloyed systems [11, 12]. Several studies of the alloy formation process during mechanical alloying have led to conflicting conclusions like the interdiffusion of elements, the interactions on interface boundaries and/or the diffusion of solute atoms in the host matrix. Indeed, the alloying process is complex and hence, involves optimization of several parameters to achieve the desired product such as type mill, raw material, milling intensity or milling speed, milling container, milling atmosphere, milling time, temperature of milling, ball-to-powder weight ratio, process control agent, etc. The formation of stable and/or metastable crystalline phases usually competes with the formation of the amorphous phase. For alloys with a negative heat of mixing, the phase formation has been explained by an interdiffusion reaction of the components occurring during the milling process [13]. Even though the number of phases reported to form in different alloy systems is unusually large [14], and property evaluations have been done in only some cases and applications have been explored, the number of investigations devoted to an understanding of the mechanism through which the alloy phase's form is very limited. This chapter summarizes the information available in this area. The obtained disordered structures by mechanical alloying are metastable and therefore, they will experience an ordering transition during heating resulting in exothermic and/or endothermic reactions. The thermal properties of materials are strongly related to the size of nanocrystals essentially when the radius of nanocrystals is smaller than 10 nm. Hence, an important task of thermal analyses is to find the size-dependent function of the thermodynamic amounts of nanocrystalline materials.

2. Thermodynamic stability

The state of a physical system evolves irreversibly towards a time-independent state in which no further macroscopic physical or chemical changes can be seen. This is the state of thermodynamic equilibrium characterized, for example, by a uniform temperature throughout the system but also by other futures. A non-equilibrium state can be defined as a state where irreversible processes drive the system towards the equilibrium state at different rates ranging from extremely fast to extremely slow. In this latter case, the isolated system may appear to have reached equilibrium. Such a system, which fulfils the characteristics of an equilibrium system but is not the true equilibrium state, is called a metastable state. Both stable and metastable states are in internal equilibrium since they can explore their complete phase space, and the thermodynamic properties are equally well defined for metastable

states as for stable states. However, only the thermodynamically stable state is in global equilibrium; a metastable state has higher Gibbs energy than the true equilibrium state.

Thermodynamically, a system will be in stable equilibrium, under the given conditions of temperature and pressure, if it is at the lowest value of the Gibbs free energy:

$$G = H - TS \tag{1}$$

Where H is enthalpy, T absolute temperature and S entropy. According to equation (1), a system can be most stable either by increasing the entropy or decreasing the enthalpy or both. At low temperatures, solids are the most stable phases since they have the strongest atomic bonding (the lowest H), while at high temperatures the -TS term dominate. Therefore, phases with more freedom of atomic movement, such as liquids and gases are most stable. Hence, in the solid-state transformations, a close packed structure is more stable at low temperatures, while a less close packed structure is most stable at higher temperatures. A metastable state is one in internal equilibrium, that is, within the range of configurations to which there is access by continuous change, the system has the lowest possible free energy. However, if there were large fluctuations (the nucleation of a more stable phase), transformation to the new phase would occur if the change in free energy, ΔG, is negative. A phase is non-equilibrium or metastable if it's Gibbs free energy is higher than in the equilibrium state for the given composition. If the Gibbs free energy of this phase is lower than that of other competing phases (or mixtures thereof), then it can exist in a metastable equilibrium. Consequently, non-equilibrium phases can be synthesized and retained at room temperature and pressure when the free energy of the stable phases is raised to a higher level than under equilibrium conditions, but is maintained at a value below those of other competing phases. Also, if the kinetics during synthesis is not fast enough to allow the formation of equilibrium phase(s), then metastable phases could form.

3. Transformation mechanism

During the mechanical alloying process, continuous fracturing, cold welding and rewelding of the powder particles lead to the reduction of grain size down to the nanometer scale, and to the increase of the atomic level strain. In addition, the material is usually under far-from-equilibrium conditions containing metastable crystalline, quasi-crystalline or amorphous phases. All of these effects, either alone or in combination, make the material highly metastable. Therefore, the transformation behaviour of these powders to the equilibrium state by thermal treatments is of both scientific and technological importance. Scientifically, it is instructive to know whether transformations in ball milled materials take place *via* the same transformation paths and mechanisms that occur in stable equilibrium phases or not. Technologically, it will be useful to know the maximal use temperature of the ball milled material without any transformation occurring and thus, losing the special attributes of this powder product. One of the most useful techniques for studying transformation behaviour of metastable phases is differential scanning calorimetry (DSC) or differential thermal analysis (DTA). Hence, a small quantity of the powder milled for a given time is heated at a

constant rate to high temperatures under vacuum or in an inert atmosphere to avoid oxidation. Depending on the phase transformations, DSC/DTA scans exhibit endothermic and/or exothermic peaks related to absorption or evolution of heat, respectively, as shown in Fig. 1.

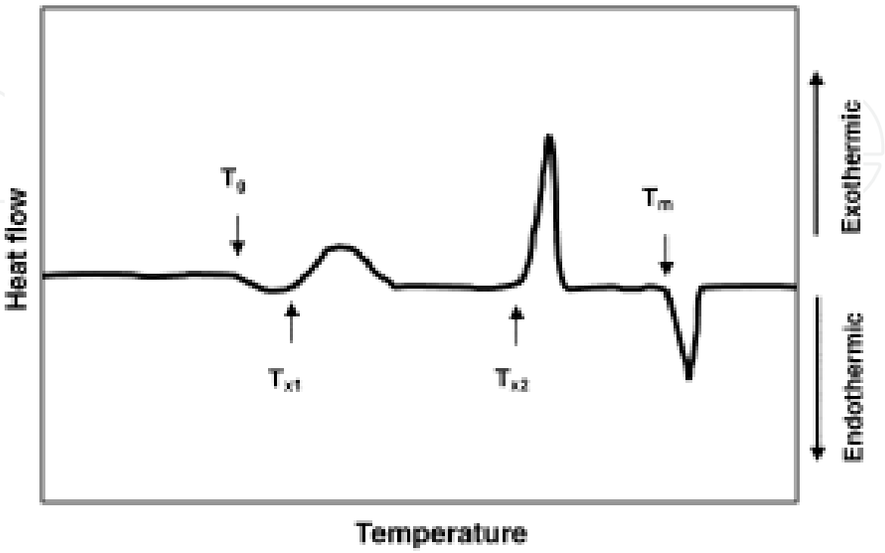

Figure 1. A schematic DSC curve depicting the different stages during crystallization of an amorphous phase where Tg is the glass transition temperature; T_m the melting temperature, T_{x1} and T_{x2} are the onset crystallization temperatures [15].

The values of the peak onset temperature and peak areas depend on the position of the baseline. Therefore, the accurate baseline can be obtained by heating the sample to the desired temperature, then cooled it back to the ambient temperature and then reheated it to higher temperatures. The second DSC scan could be used either as the baseline or subtracted from the first scan to obtain the accurate peak positions and areas. There are two types of transformations: reversible and irreversible. For the former, the product phase will revert back to the parent phase. For example, transformation from one equilibrium phase to another on heating gives rise to an endothermic peak during melting and exothermic peak during cooling. However, during irreversible transformation of metastable phases such as amorphous phases, a peak of the opposite sign is not observed. In fact, there will be no peak at all. Furthermore, because metastable phases are always more energetic than the corresponding equilibrium phases, they often exhibit exothermic peaks in the DSC/DTA curves. If an amorphous alloy powder is heated to higher temperatures, one expects to observe a broad exothermic reaction at relatively low temperatures related to structural relaxation of the amorphous phase, a glass transition temperature as well as one or more exothermic peaks corresponding to crystallization event at higher temperatures. Structural changes that occur during crystallization can be investigated by X-rays diffraction or Mössbauer spectrometry by quenching the sample from a temperature just above the DSC/DTA peak temperature. Transmission electron microscopy investigations can also be conducted to uncover the microstructural and crystal structure changes on a finer scale. In addition, compositional changes can be detected. It may be pointed out, however, that there

have not been many detailed crystallization studies of amorphous alloys synthesized by the mechanical alloying process [16].

3.1. Non-isothermal transformation

The crystallization temperature corresponds to the maximum of the exothermic peak,T_p and it increases with increasing heating rate. A relation between heating rate β and position of the transformation peak T_p first described by Kissinger [17], has been extensively used to determine the apparent activation energy for crystallization E_a:

$$\ln\frac{\beta}{T_p^2} = \left(-\frac{E_a}{RT_p}\right) + A \tag{2}$$

Where A is a constant and R is the universal gas constant. The activation energy E_a can be calculated from the slope $\left(\frac{AE_a}{R}\right)$ of the plot $\left(\frac{\beta}{T_p^2}\right)$ against $\left(\frac{1}{T_p}\right)$. Further informations about the transformation temperatures, the number of stages in which the transformation is occurring, details about the product(s) of each individual transformation (crystal structure, microstructure and chemical composition), and the activation energy (and also the atomic mechanism) can be obtained with the combination of DSC/DTA and X-rays diffraction/transmission electron microscopy techniques. The Kissinger method may not be useful in all studies of decomposition. For example, it may not be applicable for metallic glasses which may decompose by nucleation/growth, or a combination of both processes, where the decomposition is seldom described by first-order reaction kinetics [18, 19]. Solid state reactions sometimes exhibit first-order kinetics, this is one form of the Avrami-Erofeev equation (n=1). Such kinetic behaviour may be observed in decompositions of fine powders if particle nucleation occurs on a random basis and growth does not advance beyond the individual crystallite nucleated. The physical interpretation of E_a depends on the details of nucleation and growth mechanisms, and in some cases equation (2) is not valid. For each crystallization peak, the calorimetric results can be explained using the Johnson-Mehl-Avrami-Erofe'ev kinetics equation [20] for the transformed fraction:

$$\frac{dx}{dt} = K(T)f_n(x) \tag{3}$$

With:

$$f_n(x) = n(1-x)\{-\ln(1-x)\}^{(n-1)/n} \tag{4}$$

$f_n(x)$ gives the transformation rate at time t and temperature T in terms of the rate constant:

$$K(T) = k_0 exp(E/RT) \tag{5}$$

k_0 is the pre-exponential factor; E is the effective activation energy and n is the kinetic exponent. According to the Avrami exponent value, the reaction may be three-dimensional, interface-controlled growth with constant nucleation rate (n=4); three-dimensional, interface-controlled growth with zero nucleation rate (n=3) or diffusion-controlled with growth and segregation at dislocations (n=2/3)[21].

3.2. Isothermal transformation

Isothermal transformation kinetics study at different temperatures can be conducted by the Kolmogorov-Johnson-Mehl-Avrami formalism [22-25] in which the fraction transformed, x, exhibits a time dependence of the form:

$$x(t) = 1 - \exp(-kt)^{\mathrm{n}} \tag{6}$$

Where n is the Avrami exponent that reflects the nucleation rate and/or the growth mechanism; $x(t)$ is the volume of transformed fraction; t is the time, and k is a thermally-activated rate constant. The double logarithmic plot $\ln(-\ln(1-x))$ against $\ln t$ should give a straight line, the slope of which represents the order of reaction or Avrami parameter n. The rate constant k is a temperature-sensitive factor $k = k_0 exp(AE_a/RT)$, where E_a is the apparent activation energy and k_0 a constant. $x(t)$ corresponds to the ratio between the area under the peak of the isothermal DSC trace, at different times, and the total area. Such analysis was conducted on the phase transformation mechanisms in many mechanically alloyed powders since the milling process occurs at ambient temperature for different milling durations [26-31]. If the Kolmogorov-Johnson-Mehl-Avrami analysis is valid, the value of n should not change with either the volume fraction transformed, $\mathrm{V_f}$ or the temperature of transformation. Calka and Radlinski [32] have shown that the usual method of applying the Kolmogorov-Johnson-Mehl-Avrami equation and calculating the mean value of Avrami exponent over a range of volume fraction transformed, may be inappropriate, even misleading, if competing reactions or changes in growth dimensionality occur during the transformation progress. Also, a close examination of the Avrami plots reveals that there are deviations from linearity over the full range of volume fraction transformed [33]. The first derivative of the Avrami plot $\delta\,[\ln(-\ln(1-n))]/\delta \ln t$ against the volume fraction transformed [34], which effectively gives the local value of n with V_f, seems to be more sensitive. Such a plot allows a more detailed evaluation of the data and can emphasize changes in reaction kinetics during the transformation process.

4. Mechanical alloying process

Mechanical alloying has received a great interest in developing different material systems. It is a solid state process that provides a means to overcome the drawback of formation of new alloys starting from mixture of low and/or high melting temperature elements. Mechanical alloying is a ball milling process where a powder mixture placed in the vials is subjected to high-energy collisions from the balls. The two important processes involved in ball milling are fracturing and cold welding of powder particles in a dry high energy ball-mill. The alloying process can be carried out using different apparatus such as planetary or horizontal mills, attrition or spex shaker mill. The elemental or prealloyed powder mixture is charged in the jar (or vial) together with some balls. As a result of the induced heavy plastic deformation into the powder particles during the milling process, nanostructured materials are produced by the structural decomposition of coarser-grained structure. This leads to a continuous refinement of the internal structure of the powder particles down to nanometer scales.

Depending on the microstructure, the mechanical alloying process can be divided into many stages: initial, intermediate, final and complete [35]. Since the powder particles are soft in the early stage of milling, so they are flattened by the compressive forces due to the collisions of the balls. Therefore, both flattened and un-flattened layers of particles come into intimate contact with each other leading to the building up of ingredients. A wide range of particle sizes can be observed due to the difference in ductility of the brittle and ductile powder particles. The relatively hard particles tend to resist the attrition and compressive forces. However, if the powder mixture contains both ductile and brittle particles (Fig. 2a), the hard particles may remain less deformed while the ductile ones tend to bind the hard particles together [10, 36]. Cold welding is expected to be predominant in fcc metals (Fig. 2b) as compared to fracture in bcc and hcp metals (Fig. 2c).

During the intermediate stage of milling, significant changes occur in the morphology of the powder particles. Greater plastic deformation leads to the formation of layered structures (Fig. 2d). Fracturing and cold welding are the dominant milling processes. Depending on the dominant forces, a particle may either become smaller in size through fracturing or may agglomerate by welding as the milling process progresses. Significant refinement in particle size is evident at the final stage of milling. Equilibrium between fracturing and cold welding leads to the homogeneity of the particles at the macroscopic scale as shown in Fig. 2d for the $Fe_{50}Co_{50}$ powder mixture [37, 38]. True alloy with composition similar to the starting constituents is formed at the completion of the mechanical alloying process (Fig. 2e) as evidenced by the energy dispersive X analysis, EDX, (Fig. 2f). The large plastic deformation that takes place during the milling process induces local melting leading to the formation of new alloys through a melting mechanism and/or diffusion at relatively high temperature.

Mechanical alloying is a non-equilibrium process resulting in solid state alloying beyond the equilibrium solubility limit. Several studies of the alloy formation process during mechanical alloying have led to conflicting conclusions such as the interdiffusion of elements, the interactions on interface boundaries and/or the diffusion of solute atoms in the host matrix. Indeed, Moumeni et al. have reported that the FeCo solid solution was formed by the interdiffusion of Fe and Co atoms with a predominance of Co diffusion into the Fe matrix according to the spectrometry results [37]. However, Brüning et al. have shown that the FeCo solid solution was formed by the dissolution of Co atoms in the Fe lattice [39]. Sorescu et al. [40] have attributed the increase of the hyperfine magnetic field to a progressive dissolution of Co atoms in the bcc–Fe phase. Such discrepancies have been attributed to the milling conditions and/or to the fitting procedure of the Mössbauer spectra. The role of grain boundaries, the proportions and the thickness of which are dependent on the milling energy affect thus, the hyperfine structure originating some misinterpretations.

Diffusion in mechanical alloying differs from the steady state diffusion since the balance of atom concentration at the interface between two different components may be destroyed by subsequent fracturing of the powder particles. Consequently, new surfaces with different compositions meet each other to form new diffusion couples when different powder particles are cold welded together. Large difference in composition at the interface therefore promotes interdiffusion. In addition, the change in temperature during the milling process

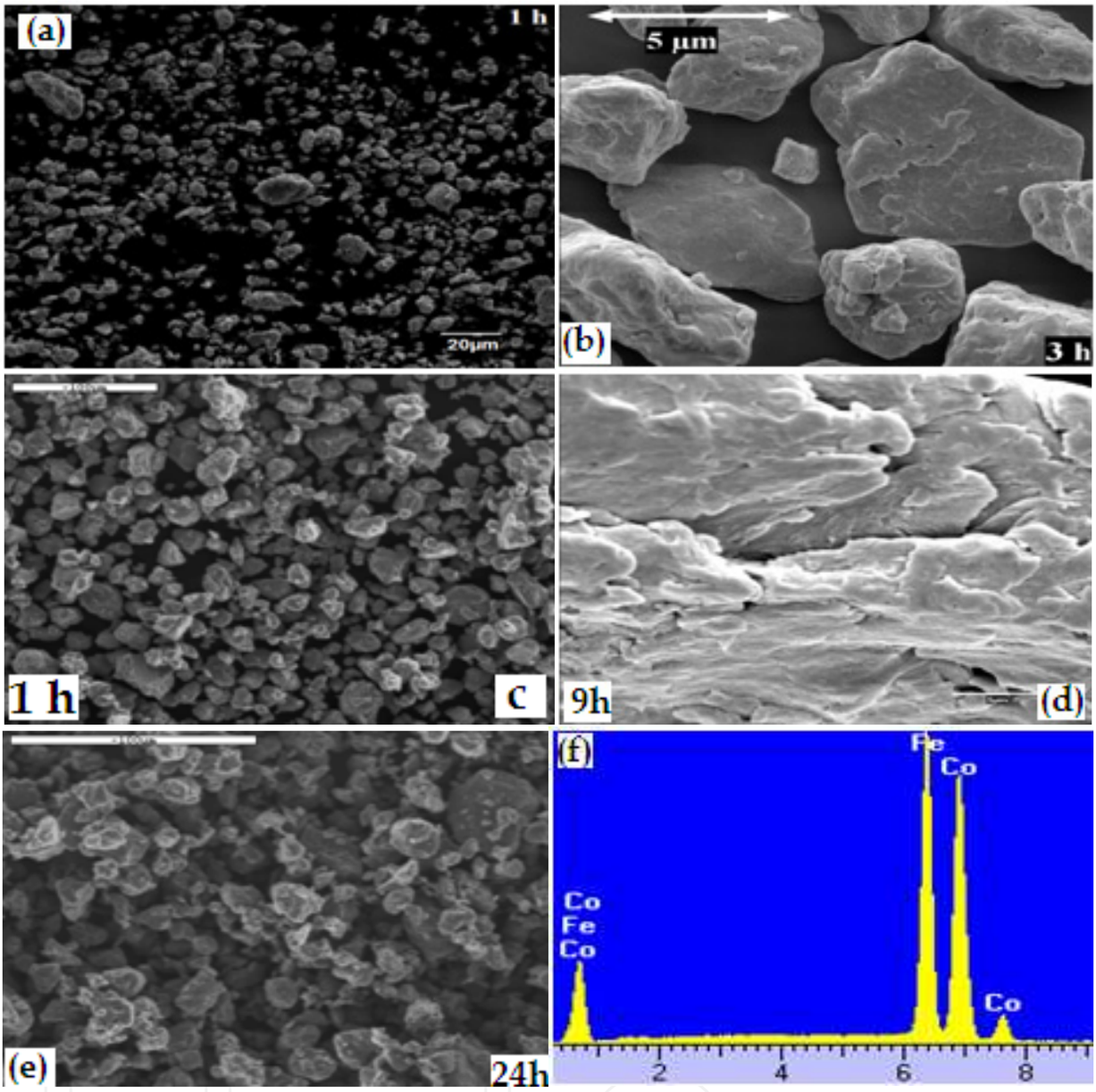

Figure 2. Morphologies of powder particles of the ball-milled $Fe_{75}Si_{15}B_{10}$ (a), $Ni_{20}Co_{80}$ (b), $Fe_{57}Cr_{31}Co_{12}$ (c and d), and $Fe_{50}Co_{50}$ powders (e) with the corresponding EDX analysis (f).

is very significant due to the exothermic reaction causing local combustion. Two major phenomena can contribute to the increase in milling temperature: friction during collisions and localized plastic deformation. At low temperatures, surface diffusion dominates over grain boundary and lattice diffusion. As the temperature is increased, however, grain boundary diffusion predominates, and at higher temperature lattice diffusion becomes the principal mode of diffusion. The first key factor controlling the formation of new alloys is the activation energy which is related to the formation of defects during balls-powder-balls and/or balls-powder-vials collisions. The second key is the vial temperature which is associated with plastic deformation as well as sliding between powder particles and high energetic balls and powder particles. The third key is the crystallite size that is related to the formation of nanometer crystalline structure during the milling process.

5. Experimental section

Mechanical alloying process was used to prepare nanocrystalline and/or amorphous alloys such as Fe, Fe-Co, Fe-Co-Nb-B, Fe-P and Ni-P from pure elemental powders in high-energy planetary ball-mills Fritsch Pulverisette P7 and Retsch PM 400/2, and vibratory ball-mill spex 8000. The milling process was performed at room temperature, under argon atmosphere, with different milling conditions such as rotation speed, ball-to-powder weight ratio, milling time and composition. In order to avoid the temperature increase inside the vials, the milling process was interrupted for 15–30 min after each 30–60 min depending on the raw mixture.

Particles powder morphology evolution during the milling process was followed by scanning electron microscopy. Structural changes were investigated by X-ray diffraction in a (θ–2θ) Bragg Brentano geometry with Cu-K$_\alpha$ radiation (λ_{Cu}=0.15406 nm). The microstructural parameters were obtained from the refinement of the X-rays diffraction patterns by using the MAUD program [41, 42] which is based on the Rietveld method. Differential scanning calorimetry was performed under argon atmosphere. Magnetic and hyperfine characterizations were studied by vibrating sample magnetometer and Mössbauer spectrometry, respectively.

6. Fe and FeCo-based alloys

6.1. Fe and Fe-Co powders

Fe and $Fe_{50}Co_{50}$ were prepared by mechanical alloying from pure elemental iron and cobalt powders in a planetary ball mill Fritsch P7, under argon atmosphere, using hardened steel vials and balls. The milling intensity was 400 rpm and the ball-to-powder weight ratio was 20:1. A disordered bcc FeCo solid solution is obtained after 24 h of milling (Fig 3), having a lattice parameter, a = 0.2861(5) nm, larger than that of the coarse-grained FeCo phase (a = 0.2825(5) nm). Such a difference in the lattice parameter value may be due to heavily cold worked and plastically deformed state of the powders during the milling process, and to the introduction of several structural defects (vacancies, interstitials, triple defect disorder, etc.).

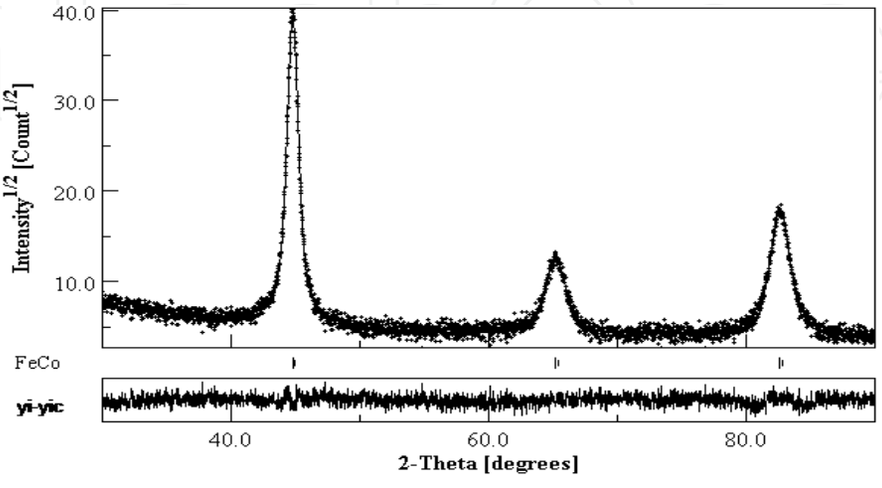

Figure 3. Rietveld refinement of the XRD pattern of the $Fe_{50}Co_{50}$ powders milled for 40 h [7].

With increasing milling time, the crystallite size decreases down to the nanometer scale and the internal strain increases. The double logarithmic plot of the crystallite size versus milling time exhibits two-stage behaviour for both Fe and $Fe_{50}Co_{50}$ powders (Fig. 4). A linear fit gives slopes of –0.65 and –0.20 for short and extended milling times, respectively, in the case of Fe; and slopes of –0.85 and –0.03, respectively, for short and extended milling times in the case of $Fe_{50}Co_{50}$ mixture. The critical crystallite size achievable by ball milling is defined by the crossing point between the two regimes with different slopes [43]. Consequently, the obtained critical crystallite sizes are of about 13.8 and 15 nm for Fe and $Fe_{50}Co_{50}$ powders, respectively. By using different milling conditions (mills type, milling intensity and temperature) to prepare nanostructured Fe powders, Börner et al. have obtained the two-regime behaviour, for the grain refinement by using the Spex mill, with slopes of –0.41 and –0.08 for short and extended milling times, respectively. However, the crystallite sizes show only a simple linear relation with slopes of –0.265 and –0.615 by using the Retsch MM2 shaker and the Misuni vibration mill, respectively. The obtained critical crystallite size value was 19 nm [44].

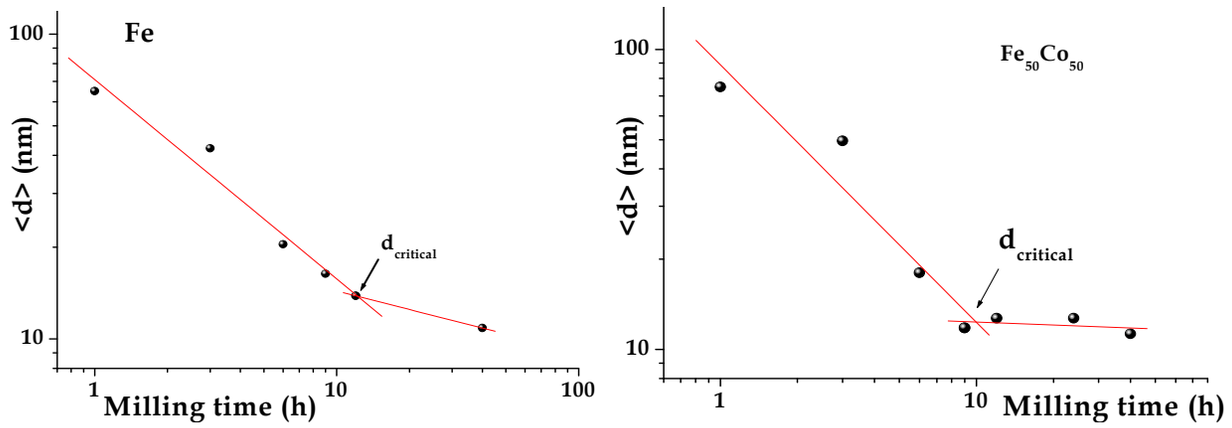

Figure 4. Double logarithmic plot of the crystallite size against milling time for nanostructured Fe and $Fe_{50}Co_{50}$ powders [7].

DSC scans of nanostructured Fe and $Fe_{50}Co_{50}$ powders milled for 40 h are shown in Fig. 5. The non-equilibrium state is revealed by the broad exothermic reaction for both samples, in the temperature range 100–700°C, which is consistent with the energy release during heating due to recovery, grain growth and relaxation processes. As a result of the cold work during the milling process, the main energy contribution is stored in the form of grain boundaries and related strains within the nanostructured grains which are induced through grain boundary stresses [45]. It has been reported that the stored energies during the alloying process largely exceed those resulting from conventional cold working of metals and alloys. Indeed, they can achieve values typical for crystallization enthalpies of metallic glasses corresponding to about 40% of the heat of fusion, ΔH_f [45]. The major sources of mechanical energy storage are both atomic disorder and nanocrystallite boundaries because the transition heats evolving in the atomic reordering and in the grain growth are comparable in value [46].

For the nanostructured Fe powders, the first endothermic peak is linked to the bcc ferro-paramagnetic transition temperature, T_C, and the second peak to the bcc→fcc transition

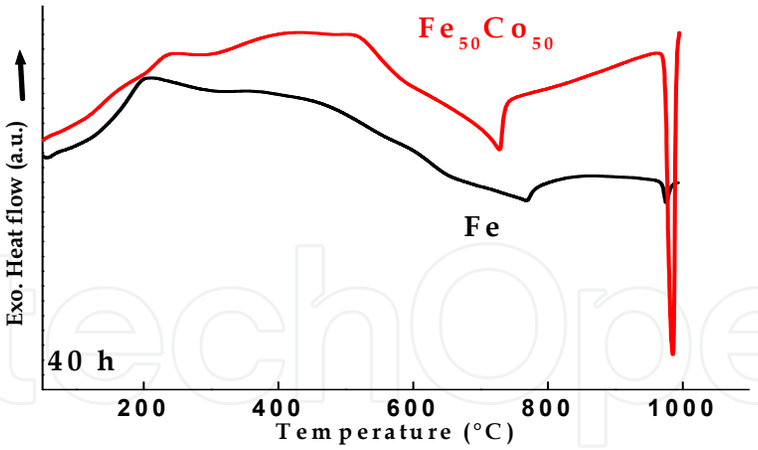

Figure 5. DSC scans of nanostructured Fe and $Fe_{50}Co_{50}$ powders milled for 40 h [7].

temperature, $T_{\alpha\rightarrow\gamma}$. The depression of Curie temperature with increasing milling duration (Fig. 6), which is ascribed to changes in local order, indicates that the nearest-neighbour coordination is essentially changed in the magnetic nanocrystallites. This reflects to some extent that there are more open disordered spaces or the nearest–neighbour coordination distance in the nanometer sized crystallites is increased, caused by lattice distortion. In fact, if the crystallite sizes are small enough, the structural distortions associated with surfaces or interfaces can lower the Curie temperature. This can be correlated to the increase of the lattice parameter and its deviation from that of the perfect crystal. It has been reported on far-from-equilibrium nanostructured metals, that interfaces present a reduced atomic coordination and a wide distribution of interatomic spacing compared to the crystals and consequently, the atomic arrangement at the grain boundary may be considered close to the amorphous configuration and should therefore alter the Curie temperature. The most reported values of Tc do not deviate strongly from that of the bulk materials. For example, the Tc of 360°C for Ni[C] nanocrystals is in good agreement with that of bulk Ni [47]. Host et al. have reported a Tc value of 1093°C for carbon arc produced Co[C] nanoparticles, in good agreement with the 1115°C value for bulk Co [48]. The Curie temperature of 10 nm Gd is

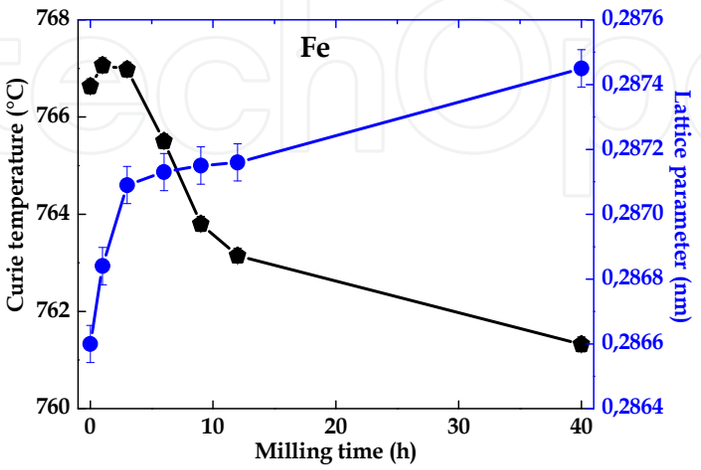

Figure 6. Evolution of the Curie temperature and the lattice parameter of the Fe powders as a function of milling time [7].

decreased by about 10 K from that of coarse-grained Gd while the magnetic transition is broader [49]. According to both Tc and $T_{\alpha\to\gamma}$ temperature values, the paramagnetic nanostructured bcc α–Fe domain is extended by about 50°C at the expense of both magnetic bcc α–Fe and nonmagnetic fcc γ–Fe as compared to coarse-grained bcc α–Fe.

The disorder-order phase transformation temperature of the nanostructured FeCo powders which is nearly constant (~724°C) along of the milling process (Fig. 7), is comparable to that of bulk Fe-Co alloys. It is commonly accepted that Fe-Co undergoes an ordering transition at around 730°C, where the bcc structure takes the ordered α'–CsCl(B2)-type structure [50]. The ordering effect in the FeCo nanocrystals has been revealed by the changes in the magnetization upon heating and the temperature variation of the coercivity on heating and cooling [51]. Also, the phase transformation temperature from bcc–α to fcc–γ structure in the $Fe_{50}Co_{50}$ powders is rather milling time independent (~982°C). The lower resistivity of $Fe_{50}Co_{50}$ compared to that of pure Fe at 300 K [52] and the higher Curie temperature of $Fe_{50}Co_{50}$ suggest that there is less scattering of the conduction electrons by the magnetic excitations. Thus, the Curie temperature cannot be clearly observed because there is a phase transformation from the bcc to fcc form at 985°C.

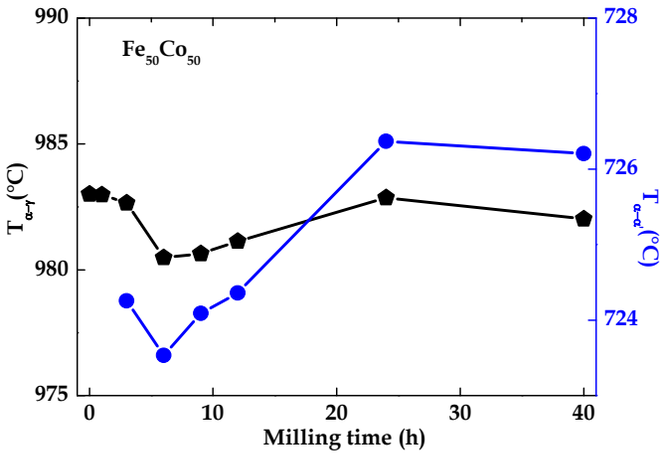

Figure 7. Evolution of the order-disorder, $T_{\alpha\to\alpha'}$ and the bcc→fcc, $T_{\alpha\to\gamma}$, temperatures of the $Fe_{50}Co_{50}$ powders as a function of milling time [7].

6.2. Fe-Co-Nb-B powders

Nanostructured and disordered structures obtained by mechanical alloying are usually metastable. Depending on the Nb and B contents, the mechanically alloyed Fe-Co-Nb-B powders structure may be partially amorphous either magnetic and/or paramagnetic. Pure elemental powders of iron (6-8 μm, 99.7%), cobalt (45 μm, 99.8%), niobium (74 μm, 99.85%) and amorphous boron (> 99%) were mixed to give nominal compositions of $Fe_{57}Co_{21}Nb_7B_{15}$ and $Fe_{61}Co_{21}Nb_3B_{15}$ (wt. %), labelled as 7Nb and 3Nb, respectively. The milling process was performed in a planetary ball-mill Fritsch Pulverisette 7, under argon atmosphere, using hardened steel balls and vials. The ball-to-powder weight ratio was about 19/2 and the rotation speed was 700 rpm. For the $(Fe_{50}Co_{50})_{62}Nb_8B_{30}$ mixture, the milling process was performed in a planetary ball-mill Retsch PM400/2, with a ball-to-powder weight ratio of

about 8:1 and a rotation speed of 350 rpm. In order to avoid the increase of the temperature inside the vials, the milling process was interrupted after 30 min for 15 min.

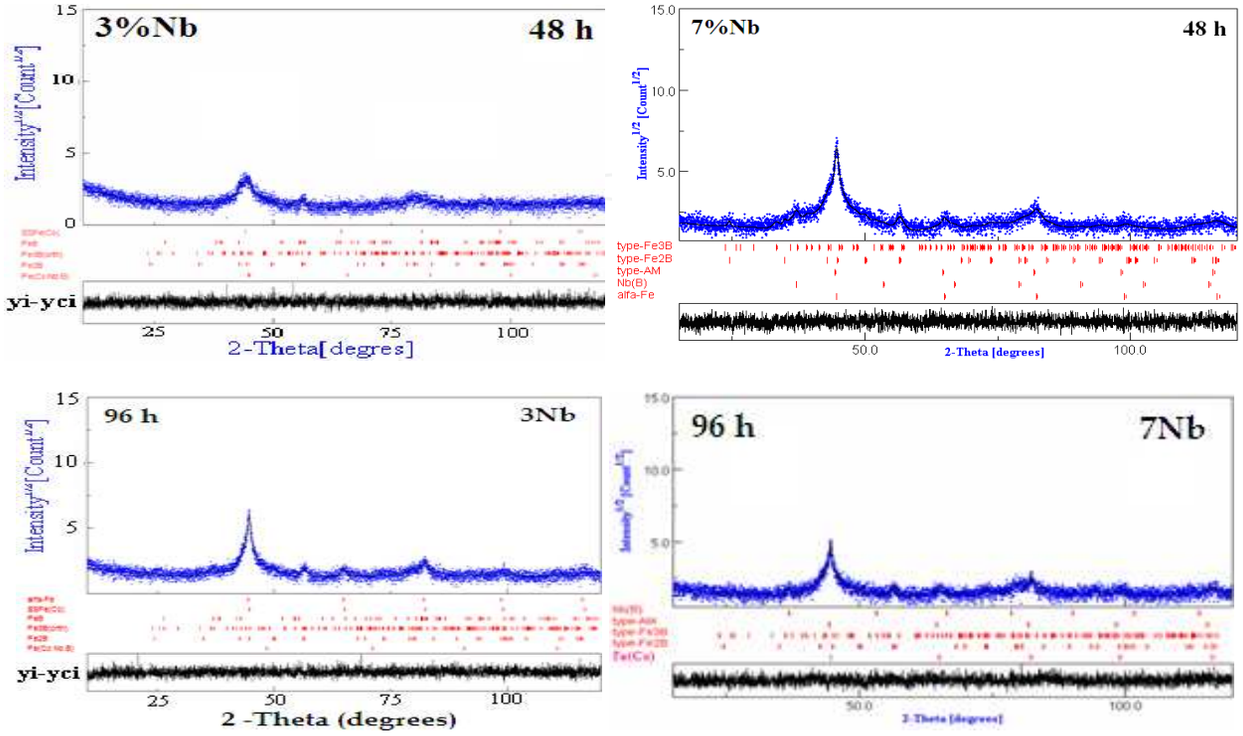

Figure 8. Rietveld refinement of the XRD patterns of 7Nb and 3Nb powders milled for 48 and 96 h [53, 54].

The XRD patterns of 7Nb and 3Nb mixtures milled for 48 h (Fig. 8) are consistent of a large number of overlapping diffraction peaks related to different phases. The Rietveld refinement reveals the formation of a partially amorphous structure of about ~78%, where nanocrystalline tetragonal–Fe_2B, tetragonal–Fe_3B and bcc–FeCo type phases were embedded for 3Nb powders [53]. Whereas, for 7Nb powders, the milling product is a mixture of amorphous (~73.6%), bcc–Nb(B), tetragonal–Fe_2B, orthorhombic–Fe_3B and bcc FeCo type phases [54]. Further milling (up to 96 h) leads to the increase of the amorphous phase proportion for 7Nb and the mechanical recrystallization in the case of 3Nb mixture (Fig. 8) as evidenced by the decrease and the increase of the diffraction peaks intensity, respectively. The formation of the amorphous phase is confirmed by the Mössbauer spectrometry results as shown in Fig. 9. After 48 h of milling, the Mössbauer spectra exhibit more or less sharp absorption lines superimposed upon a broadened spectral component assigned to the structural disorder of the amorphous state [55]. For 3Nb powders, the mechanical recrystallization is confirmed by the emergence of sharp sextet related to the primary crystallization of α–Fe and FeCo after 96 h of milling. However, a stationary state is achieved for 7Nb powders. The increase of the average hyperfine magnetic field, $< B_{hyp} >$, from 19.18 to 23.14 T after 96 h of milling of 3Nb powders is correlated to the decrease/increase of the amorphous/nanocrystalline relative area. The nanocrystalline (NC) component consists of Fe sites with B_{hyp}>31 T and the interfacial (IF) one is related to the nanostructured Fe–borides with B_{hyp} ranged from 24 to 30 T [28, 56, 57].

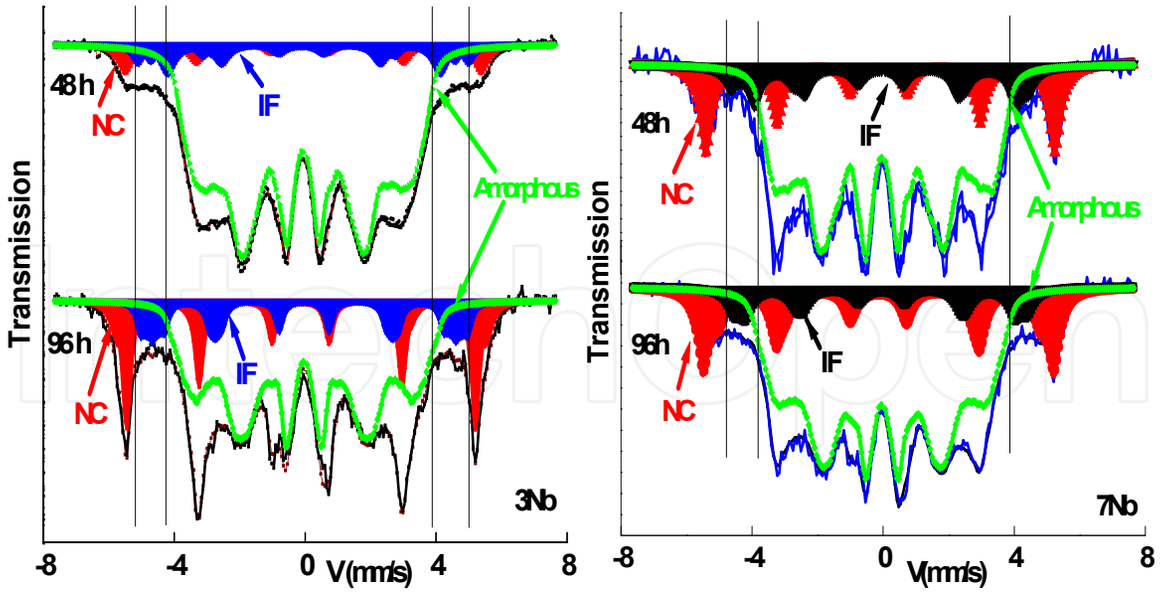

Figure 9. Room temperature Mössbauer spectra of 3Nb and 7Nb powders milled for 48 and 96 h [55].

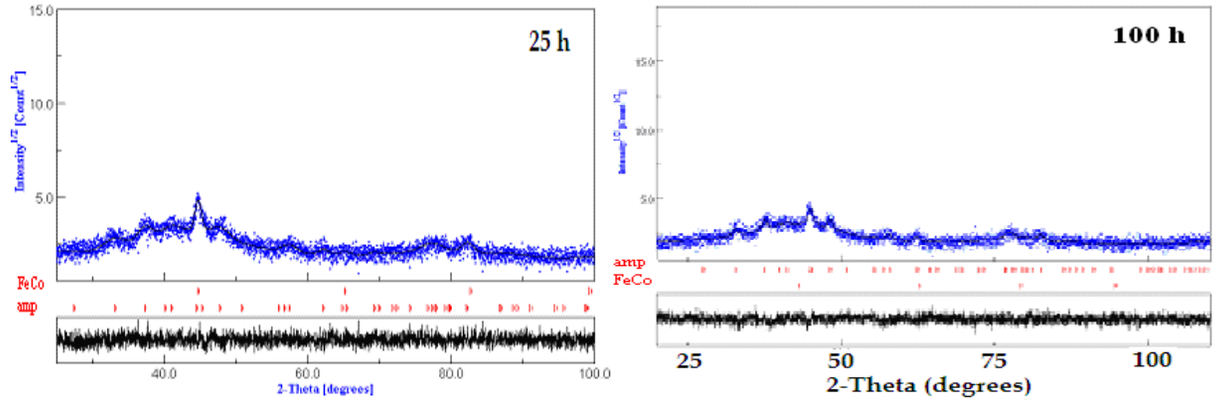

Figure 10. XRD patterns of the $(Fe_{50}Co_{50})_{62}Nb_8B_{30}$ powders milled for 25 and 100 h.

For the $(Fe_{50}Co_{50})_{62}Nb_8B_{30}$ powders mixture milled for 25 and 100 h, the best Rietveld refinements of the XRD patterns were obtained with two components: bcc–FeCo and amorphous phase (Fig. 10). The complete transformation of the heavily deformed FeB and bcc FeCo type phases into an amorphous state is achieved, after 125 h of milling, through the mechanically enhanced solid-state amorphization which requires the existence of chemical disordering, point defects (vacancies, interstitials) and lattice defects (dislocations). Indeed, the severe plastic deformation strongly distorts the unit cell structures making them less crystalline. The powder particles are subjected to continuous defects that lead to a gradual change in the free energy of the crystalline phases above those of amorphous ones, and hence to a disorder in atomic arrangement. The Mössbauer spectra confirm the formation of a paramagnetic amorphous structure, where about 3.8% of FeCo and Fe_2B nanograins are embedded, after 125 h of milling (Fig. 11).

Nanocrystalline $Fe_{72.5}Co_{7.5}Nb_{5+x}B_{15-x}$ with x=0, 5 and 10 at.% labelled as A, B and C, respectively, were prepared by mechanical alloying from pure elemental powders in a planetary ball-mill Retsch PM400, under argon atmosphere, using stainless steel balls and

vials. The ball-to-powder weight ratio was about 8:1 and the rotation speed was 200 rpm [58]. The crystallite size decreases with increasing milling duration to about (7.1 ± 0.3) nm for the B-richest alloy (A). The XRD patterns (Fig. 12) reveal the formation of a bcc Fe-rich solid solution after 80 h of milling having an average lattice parameter of about 0.2871 nm for the three alloys.

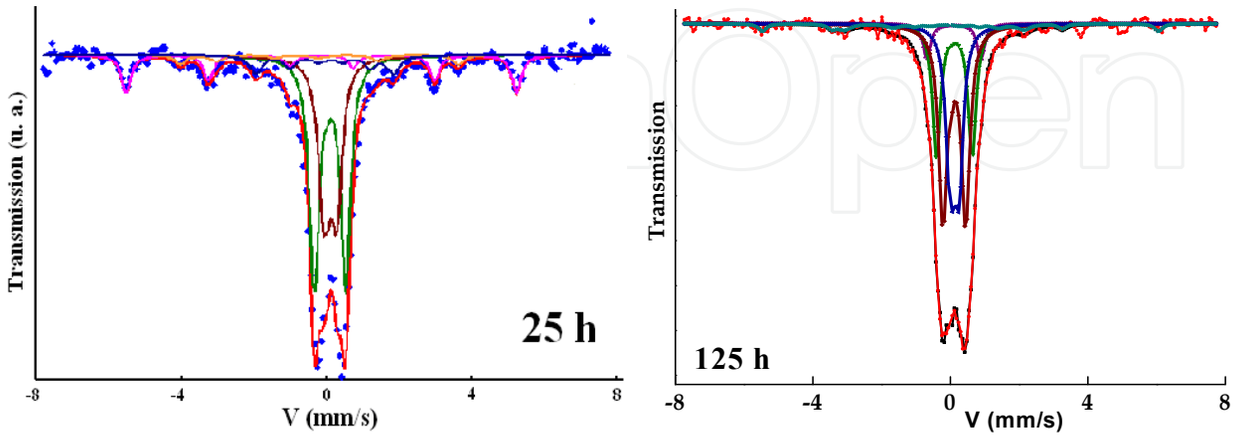

Figure 11. Room temperature Mössbauer spectra of the $(Fe_{50}Co_{50})_{62}Nb_8B_{30}$ powders milled for 25 and 125 h.

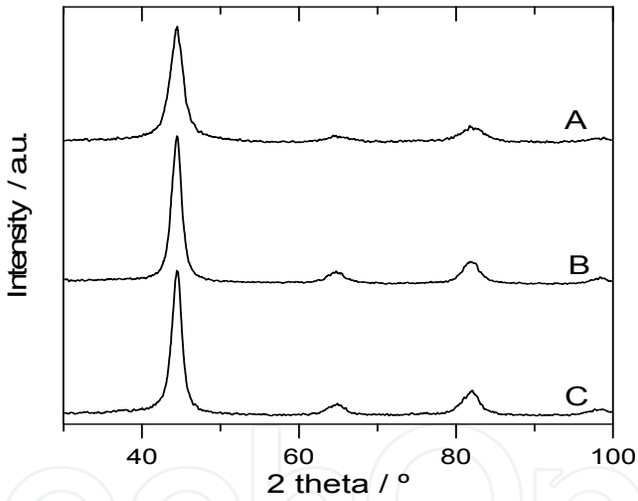

Figure 12. XRD patterns of alloys A, B and C milled for 80 h [58].

Depending on the structural state after each milling time, several exothermic and endothermic peaks appear on heating of the mechanically alloyed Fe-Co-Nb-B powders. Representative DSC scans of 7Nb and 3Nb (Fig. 13) as well as $(Fe_{50}Co_{50})_{62}Nb_8B_{30}$ powder mixtures (Fig. 14) exhibit different thermal effects (Table 1). For all ball milled powders, the first exothermic peak that spreads over the temperature range 100–300°C can be attributed to recovery, strains and structural relaxation. The important heat release (20.56 J/g) for 3Nb powders might be related to the amount of structural defects. The second exothermic peak (2), at 415°C, can be attributed to the α-Fe and/or α-FeCo primary nanocrystallization. This temperature is smaller than that obtained for the ball-milled 7Nb and $(Fe_{50}Co_{50})_{62}Nb_8B_{30}$ powders. Such a difference might be attributed to the Nb content since Co usually increases

the onset of crystallization by about 20°C because this atom inhibits atomic movement raising the kinetic barrier for crystallization. The small exothermic peaks centred at ~623.5°C (3) and ~675.7°C (4) in the 3Nb powders can be related to the crystallization of Fe-borides.

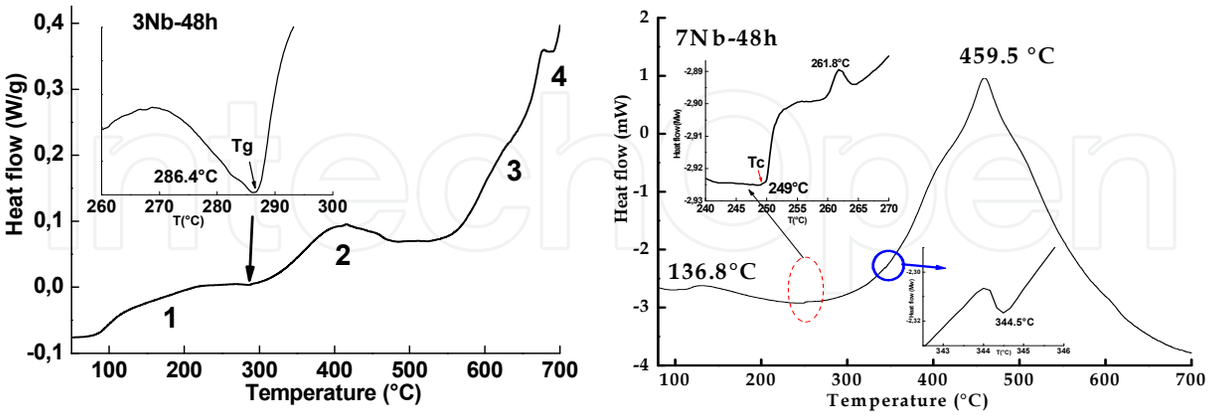

Figure 13. DSC scans of 3Nb and 7Nb powder mixtures milled for 48 h [55].

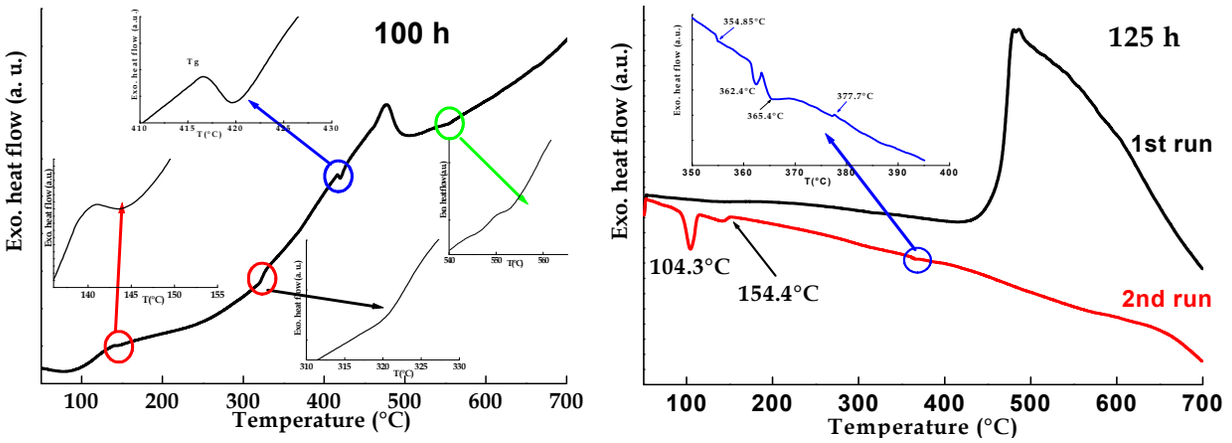

Figure 14. DSC scans of the $(Fe_{50}Co_{50})_{62}Nb_8B_{30}$ powders milled for 100 and 125 h.

Thermal stability of the nanocrystalline phases was investigated by DSC for alloys A, B and C milled for 160 h at a heating rate of 10 K/min (Fig. 15). The broad exothermic process starting at ~400–420 K is due to early surface crystallization (particle surface) and/or internal stress relaxation [58]. In all alloys, an additional exothermic process was detected with a peak temperature between 713 and 743 K. One observes that the peak temperature increases with increasing Nb content from 5 to 15%. This result agrees with those of the ball-milled 3Nb, 7Nb and $(Fe_{50}Co_{50})_{62}Nb_8B_{30}$ mixtures.

The endothermic peak at about 286.4, 344.5 and 420°C for 3Nb, 7Nb and $(Fe_{50}Co_{50})_{62}Nb_8B_{30}$ powders, respectively, that can be attributed to the glass transition temperature, Tg, gives evidence of the amorphous state formation. The glass transition temperature of the $(Fe_{50}Co_{50})_{62}Nb_8B_{30}$ powders increases rapidly up to 25 h of milling, and then remains nearly constant on further milling time (Fig. 16). The increase of Tg might be correlated to the amorphous phase proportion and/or to the change of its composition. The obtained low values compared to those of the amorphous ribbons with the same composition, can be linked to the heterogeneity of the ball-milled samples. The glass transition is not a first order

phase transition but a kinetic event dependent on the rearrangement of the system and experimental time scales. Therefore, the transition would be a purely dynamic phenomenon.

Sample Milling time (h)	**Peak**	**T(°C)**	**ΔH (J/g)**	**Tg (°C)**
$(Fe_{50}Co_{50})_{62}Nb_8B_{30}$ (100 h)	1	138.83	7.58	420
	2	**475.76**	**27.98**	
7Nb (48 h)	1	136.8	2.1	344.5
	2	**459.5**	**169.5**	
3Nb (48 h)	1	198.5	20.56	286.4
	2	**415.0**	**35.9**	
	3	623.5	1.4	
	4	675.7	3.9	

Table 1. Peak temperature, T_P, enthalpy release, ΔH, and glass transition temperature, Tg, of 7Nb and 3Nb powders milled for 48 h, and $(Fe_{50}Co_{50})_{62}Nb_8B_{30}$ mixture milled for 100 h [55].

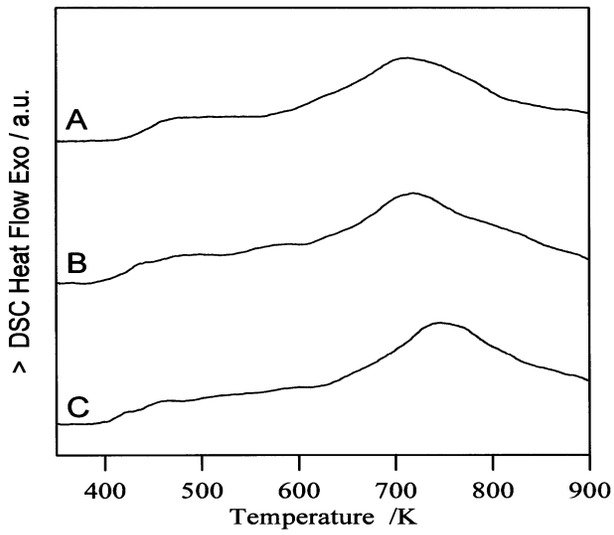

Figure 15. DSC scans at a heating rate of 10 K.min^{-1} of the ball-milled A, B and C powders for 160 h [58].

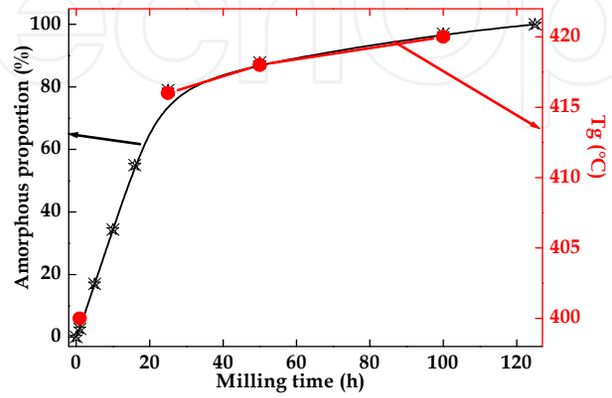

Figure 16. Variation of the glass transition temperature and the amorphous phase proportion of the $(Fe_{50}Co_{50})_{62}Nb_8B_{30}$ powders as a function of milling time.

DSC, which measures heat flow to and from a specimen relative to an inert reference, is the most common thermal analysis method used to measure the glass transition. The heat capacity step change at the glass transition yields three temperature values: onset, midpoint and endset. The midpoint is usually calculated as the peak maximum in the first derivative of heat flow (Fig. 1), although it can be calculated as the midpoint of the extrapolated heat capacities before and after the glass transition. This later is the temperature region where an amorphous material changes from a glassy phase to a rubbery phase upon heating, or *vice versa* if cooling. For example, the glass transition is very important in polymer characterization as the properties of a material are highly dependent on the relationship of the polymer end-use temperature to its Tg. In fact, an elastomer will be brittle if its Tg is too high, and the upper use temperature of a rigid plastic is usually limited by softening at Tg. Therefore, an accurate and precise measure of Tg is a prime concern to many plastics manufacturers and end use designers.

DSC detects the Curie temperature as a change in heat flow and due to the small amount of energy associated with this transition. An endothermic reaction occurs just below the Curie temperature as energy is being absorbed by the sample to induce randomization of the magnetic dipoles. An exothermic event occurs directly after the Curie temperature since no further energy is needed for randomization. Consequently, the line break at about 237°C and 249°C for 3Nb and 7Nb powders (Fig. 13), respectively, can be assigned to the ferro-paramagnetic transition at Curie temperature of the amorphous phase. Those values are comparable to that reported for the amorphous $(Fe_{100-x}Co_x)_{62}Nb_8B_{30}$ bulk metallic glasses [59], where Tc was found to be 245°C for x=0. Accordingly, one can suppose that the amorphous phase composition is Co-free FeBNb-type. Different Tc values of about (157–167)°C and (87–97)°C have been reported for the as-quenched $Fe_{52}Co_{10}Nb_8B_{30}$ and $Fe_{22}Co_{40}Nb_8B_{30}$ alloys [60], respectively. Tc of the residual amorphous phase exhibits antagonist behaviour for both alloys. It decreases with increasing crystalline fraction for the Co–rich $Fe_{22}Co_{40}Nb_8B_{30}$ alloy, and shifts to higher temperature for the Fe–rich $Fe_{52}Co_{10}Nb_8B_{30}$ alloy. Also, lower Tc values in the temperature range (214–230)°C were obtained for the as-cast state and in nanocrystalline $Fe_{77}B_{18}Nb_4Cu$ ribbons annealed at different temperatures [61].

Fig. 17 shows the evolution of Curie temperature of the amorphous phase in the $(Fe_{50}Co_{50})_{62}Nb_8B_{30}$ powders against milling time. Since the amorphous phase Curie temperature is very sensitive to the chemical composition, therefore the progressive decrease of Tc with increasing milling time can be attributed to the increase of B and/or Nb content in the amorphous matrix. It has been reported that the Curie temperature of the FeCoNbB amorphous alloys increases with the B content in the amorphous matrix [62]. Both the first and the second DSC scans of the powders milled for 100 and 125 h, respectively, display many endothermic peaks (see the inset in Fig. 14) that can be attributed to Curie temperatures of different Fe-boride phases and the residual matrix (t=125 h). For example, the endothermic peak at T=579.8°C can be related to the Curie temperature of Fe_3B [63].

The apparent activation energy of the crystallization process in the alloys A, B and C was evaluated by the Kissinger method. The obtained values 2.47±0.07, 2.63±0.05 and 2.71±0.08 eV for alloys A, B and C, respectively, can be associated with grain growth process. The

activation energy and the peak temperature variation as a function of Nb content (Fig. 18) reveal that the highest peak temperature and activation energy correspond to the 15%Nb alloy. According to the structural and thermal analysis, it can be concluded that the partial substitution of B by Nb favours the stability of nanocrystalline phase with regard to crystal growth.

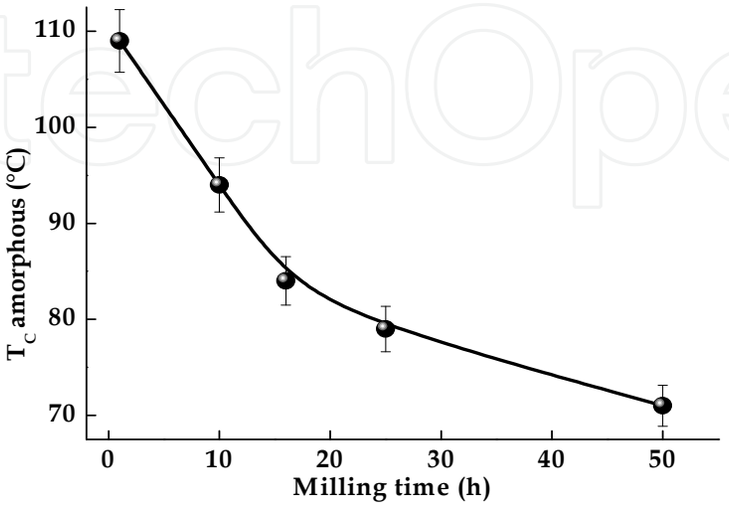

Figure 17. Variation of the amorphous phase Tc in the $(Fe_{50}Co_{50})_{62}Nb_8B_{30}$ powders as a function of milling time.

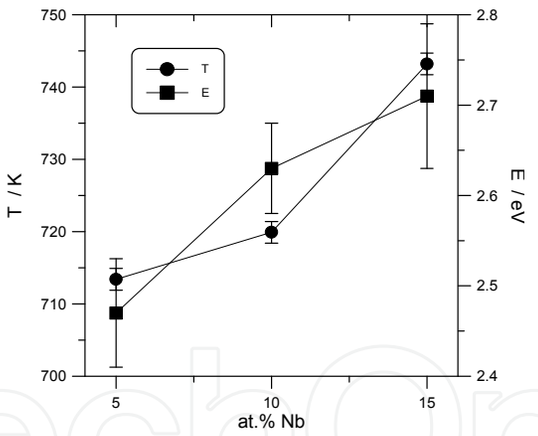

Figure 18. Apparent activation energy and peak temperature of the crystallization process against Nb content for alloys A, B and C milled for 160 h [58].

Stability of the nanostructured Fe-Co-Nb-B powders can be followed by the variation of the magnetic properties such as saturation magnetization, Ms, and coercivity, Hc. The hysteresis loops of ball milled 3Nb powders for 48 h and 7Nb powders for 96 h and heat treated up to 700°C (Fig. 19) display a sigmoidal shape which is usually observed in nanostructured samples with small magnetic domains. This can be correlated to the presence of structural distortions inside grains. One notes that both Ms and Hc values of 3Nb powders are higher than those of 7Nb powders. The increase of Hc from 71 to 115.5 Oe, after heat treatment of the ball milled 3Nb powders for 96 h, points out that the FeCo-rich ferromagnetic grains

might be separated by Nb and/or B-rich phase with weaker ferromagnetic properties. Another possible origin for this behaviour is the increase of Fe_2B boride proportion. Nonetheless, for 7Nb mixture Ms increases slightly while Hc remains nearly constant after heat treatment of the powders milled for 48 h. One can conclude that the nanostructured state is maintained after heat treatment.

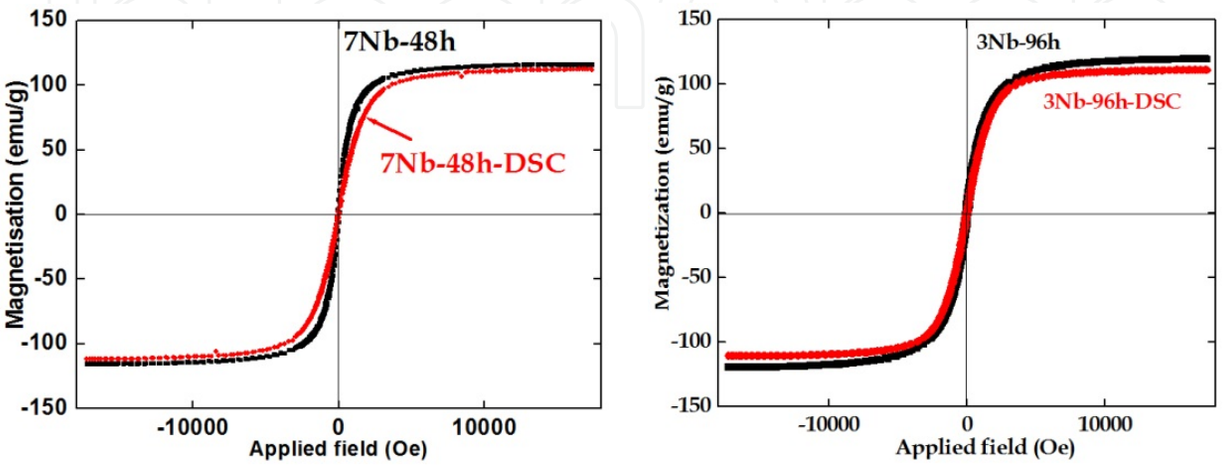

Figure 19. Hysteresis loops of 3Nb and 7Nb powders milled for 96 h and 48 h, respectively, and after heat treatment up to 700°C [55].

7. Ni-P powders

Thermal annealing leads, in general, to the relaxation of the introduced stresses during the milling process. The DSC curves of the ball-milled $Ni_{70}P_{30}$ powders for 3 and 12 h (Fig. 20) display different behaviour on heating at a rate of 10°C.min^{-1}. After the first run up to 700°C (scan a), samples are cooled down to ambient temperature, then reheated in the same conditions. One notes that the DSC signal of the second run (scan b) shows a line without any thermal effect indicating that the phase transformation is achieved during the first run [64]. However, for the first run curve, the enthalpy release spreads over the temperature range (100–650)°C. The large exothermic reactions at temperatures below 300°C can be attributed to recovery and strain relaxation. The DSC curve of the powder milled for 3 h shows a single exothermic peak at 496.4°C. While, after 12 h of milling, the DSC curve reveals several endothermic peaks, and one exothermic peak at 567.6°C. According to the Curie temperature of pure Ni (T_c = 350°C), the endothermic peaks (Fig. 21) can be related to the magnetic transition temperature of dilute Ni(P) solid solutions. However, the exothermic peak might be assigned to a growth process of Ni_2P nanophase. The depression of Tc compared to that of pure Ni indicates that the nearest-neighbour coordinates are essentially changed in the magnetic nanocrystallites by the P additions. The reason for the existence of several magnetic phase states and therefore, several Curie temperatures can be attributed to inhomogeneities since the Curie temperature is sensitive to the chemical short range order and subsequently, to the local Ni environment.

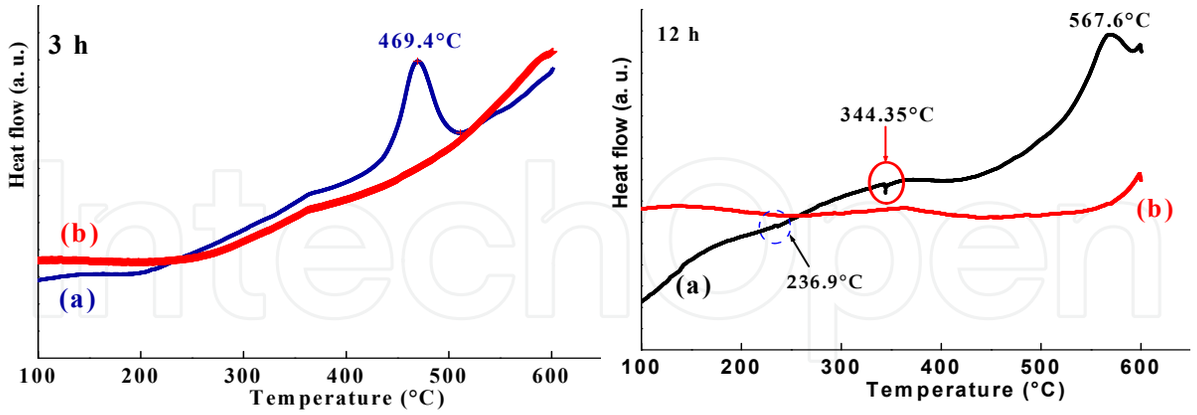

Figure 20. DSC plots of the $Ni_{70}P_{30}$ powders milled for 3 and 12 h at a heating rate of 10°C/min; first (a) and second heating runs (b) [64].

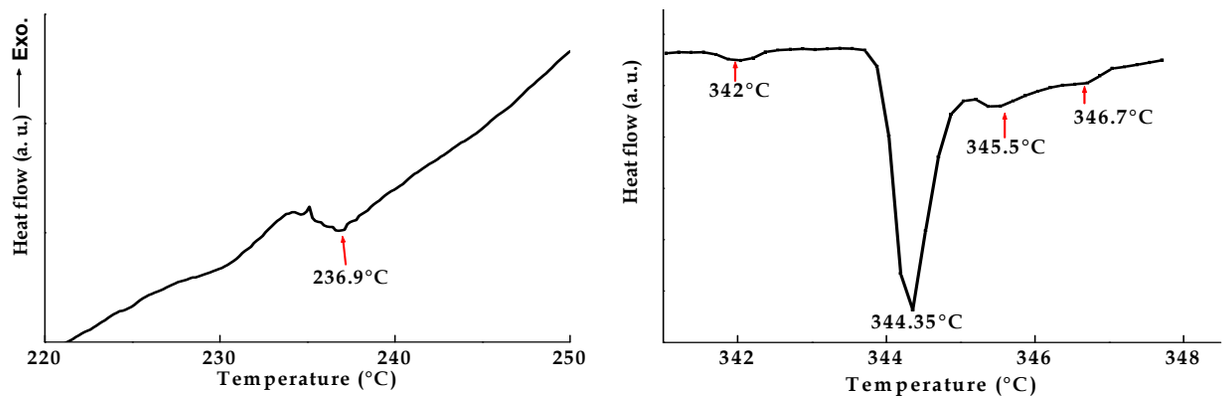

Figure 21. Enlargement of the low temperature regions of the DSC scan of the $Ni_{70}P_{30}$ powders milled for 12 h.

8. Kinetics of powder mixing

8.1. Fe-Mo mixture

The kinetics of Mo dissolution into the α-Fe matrix of the Fe-6Mo mixture has been deduced from the XRD analysis by following the evolution of the (110) diffraction peak intensity of the unmixed Mo as a function of milling time [26]. Since the milling process occurs at room temperature, one can suppose that the temperature is constant. In addition, the milling time can be considered as the necessary time for phase transformation. Consequently, the mixed fraction of Mo which is considered as the fraction transformed, x, can be described by the Johnson-Mehl-Avrami formalism. The double logarithmic plot ln(-ln(1-x)) versus lnt leads to the Avrami parameter n, and the rate constant k. Two stages have been distinguished according to the kinetics parameter values: (i) a first stage with n_1= 0.83 and k_1= 0.34; and (ii) a second stage with n_2= 0.33 and k_2 = 0.73. The former proves that the Mo dissolution is very

slow even non-existent in the early stage of milling (up to 6 h), while the later can be linked to the increased diffusivity by decreasing crystallite size and increasing the grain boundaries area on further milling time.

8.2. $Fe_{27.9}Nb_{2.2}B_{69.9}$ mixture

Amorphization kinetics of the $Fe_{27.9}Nb_{2.2}B_{69.9}$ (at. %) powders has been deduced from the Mössbauer spectrometry results by following the variation of the α-Fe transformed fraction as a function of milling time [27]. The amorphization process can be described by one stage with an Avrami parameter of about n~1 (Fig. 22). This value is comparable to those obtained for transformations controlled by the diffusion at the interface and dislocations segregation with $0.45 < n < 1.1$. This might be correlated to the existence of a high density of dislocations and various types of defects as well as to the crystallite size refinement. Comparable values of the Avrami parameter were obtained for the primary crystallization of the amorphous FeCoNbB alloy prepared by melt spinning [65].

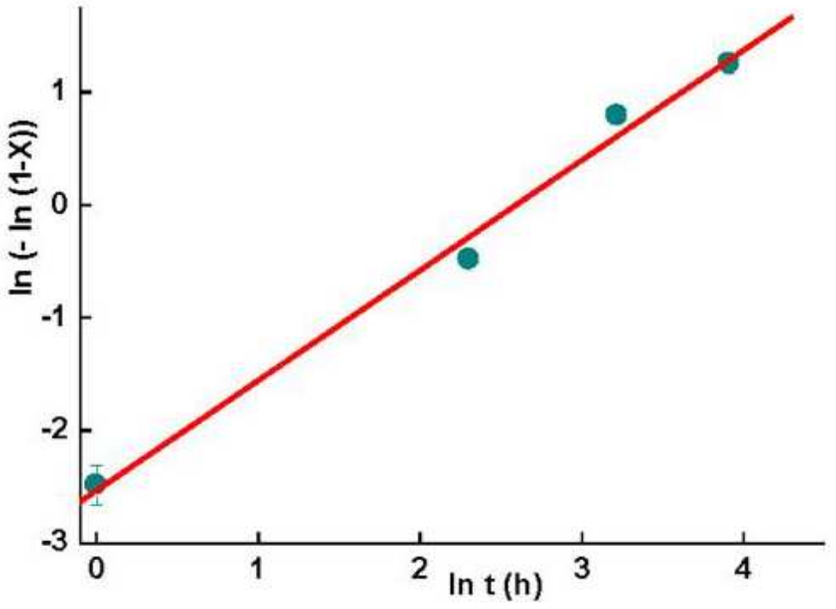

Figure 22. Johnson-Mehl-Avrami plot of the ball-milled $Fe_{27.9}Nb_{2.2}B_{69.9}$ versus milling time [28].

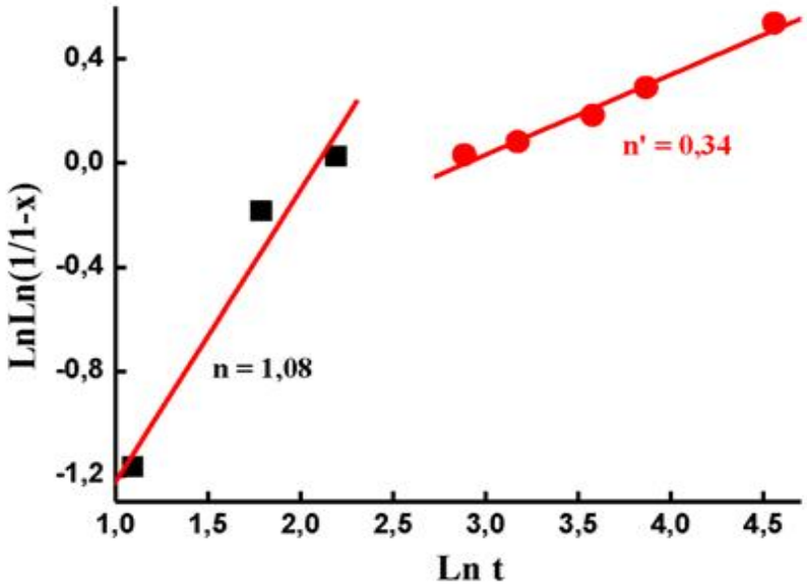

Figure 23. Johnson-Mehl-Avrami plot of the ball-milled $Fe_{57}Co_{21}Nb_7B_{15}$ versus milling time [27, 66].

8.3. FeCoNbB powders

The mixing kinetics of the $Fe_{57}Co_{21}Nb_7B_{15}$ powders can be described by two stages [27, 66] with different Avrami parameters n = 1.08 and n' = 0.34 (Fig. 23). The lower values of the Avrami parameter can be ascribed to the presence of both Nb and B which favour the grain size refinement and the formation of a highly disordered state. For the $(Fe_{50}Co_{50})_{62}Nb_8B_{30}$ mixture, two stages have been obtained with different Avrami parameter values n_1 = 1.41 and n_2 = 0.34 [2]. The former value is comparable to those obtained for the Finemet and Nanoperm [67]. However, it is higher than that obtained during the crystallization of the amorphous FeCoNbB alloy where α-(Fe,Co) nanocrystals with grain size of 15 nm are distributed in the amorphous matrix [65]. Bigot et al. have obtained a value of n = 1.5 for the nanocrystallization of the Finemet [68]. Comparable kinetics parameters have been obtained in the Ni-15Fe-5Mo (n = 1.049 and k = 0.57) [69]. The important fraction of structural defects which is introduced during the milling process favours the phase formation through the diffusion at the surface which is dominant, at lower temperatures, in comparison to the diffusion by the grain boundaries and the lattice parameter (vacancy's diffusion).

9. Conclusion

Thermal analysis is widely used in the reaction study of the mechanically alloyed powder particles because of the obtained metastable disordered structures. Hence, thermal annealing leads to the relaxation of the introduced stresses during the milling process. The heat effects are dependent on the structural and microstructural properties of the ball-milled powders.

Author details

Safia Alleg* and Saida Souilah
Badji Mokhtar Annaba University, Department of Physics, Laboratoire de Magnétisme et Spectroscopie des Solides (LM2S) B.P. 12, 23000 Annaba, Algeria

Joan Joseph Suñol
Dep. De Fisica, Universitat de Girona, Campus Montilivi, 17071 Girona, Spain

Acknowledgement

Prof. Safia Alleg is grateful to the University of Girona-spain for the financial support as invited professor. Financial support from AECID A/016051/08 and AECID A/025066/09 projects is acknowledged. Financial support from WLI Algeria is acknowledged.

10. References

[1] Suryanarayana C (2004) Mechanical alloying and milling. Marcel Dekker. 457-p
[2] Alleg S, Azzaza S, Bensalem R, Suñol JJ, Khene S, Fillion G (2009) Magnetic and structural studies of mechanically alloyed $(Fe_{50}Co_{50})_{62}Nb_8B_{30}$ powder mixtures. J. Alloys Compd. 482: 86-89.
[3] Moumeni H, Alleg S, Djebbari C, Bentayeb FZ, Greneche JM (2004) Synthesis and characterization of nanostructured FeCo alloys. J. Mat. Sci. 39: 5441-5443.
[4] Bensebaa N, Alleg S, Bentayeb FZ, Bessais L, Greneche JM (2005) Microstructural characterization of Fe-Cr-P-C powder mixture prepared by ball milling. J. Alloys Compd. 388:41-48.
[5] Bentayeb FZ, Alleg S, Bouzabata B, Greneche JM (2005) Study of alloying mechanisms of ball milled Fe-Cr and Fe-Cr-Co powders. J. Magn. Magn. Mat. 288: 282-296.
[6] Tebib W, Alleg S, Bensalem R, Greneche JM (2010) Structural study of the mechanically alloyed Fe-P powders. Int. J. Nanoparticles 3:237-244.
[7] Azzaza S, Alleg S, Moumeni H, Nemamcha AR, Rehspringer J L, Greneche J M (2006) Magnetic properties of nanocrystalline ball milled Fe and $Fe_{50}Co_{50}$ alloy. J. Phys.: Condens. Matter 18 : 7257-7272.
[8] Tebib W, Alleg S, Bensebaa N, Bentayeb FZ, Suñol JJ, Greneche JM (2008) Structural characterization of nanostructured Fe-8P powder mixture. J. Nanosci. Nanotechnol. 8:2029-2036.

* Corresponding Author

[9] Alleg Safia, Bentayeb Fatima Zohra, Djebbari Chafia, Bessais Lotfi, Greneche Jean Marc (2008) Effect of the milling conditions on the formation of nanostructured Fe-Co powders. Phys. Stat. Sol. (a) 205: 1641-1646.

[10] Alleg S, Ibrir M, Fenineche NE, Azzaza S, Suñol JJ(2010) Magnetic and structural characterization of the mechanically alloyed $Fe_{75}Si_{15}B_{10}$ powders. J. Alloys Compd. 494: 109-115.

[11] Bansal C, Gao ZQ, Hong L B, Fultz B (1994) Phases and phase stabilities of Fe_3X alloys (X=Al, As, Ge, In, Sb, Si, Sn, Zn) prepared by mechanical alloying. J. Appl. Phys. 76:5961–5966.

[12] Macrí PP, Enzo S, Cowlam N, Frattini R, Principi G, Hu WX (1995) Mechanical alloying of immiscible $Cu_{70}TM_{30}$ alloys (TM = Fe,Co). Philosophical Magazine Part B 71:249-259.

[13] Bentayeb FZ, Alleg S, Greneche J M (2007) Structural and microstructural study of Fe-31Cr-12Co mixture prepared by ball milling. J. Alloys Compd. 434: 435-477.

[14] Dekhil L, Alleg S, Suñol JJ, Greneche JM (2009) X-rays diffraction and Mössbauer spectrometry studies of the mechanically alloyed Fe-6P-1.7C powders. Adv. Pow. Technol. 20:593-597.

[15] Azzaza S (2006) Magister. Badji Mokhtar Annaba University, Algeria.

[16] Sherif El-Eskandarany M, Saida J, Inoue A (2002) Amorphization and crystallization behaviours of glassy $Zr_{70}Pd_{30}$ alloys prepared by different techniques. Acta Mater. 50:2725–2736.

[17] Kissinger HE (1957) Reaction kinetics in differential thermal analysis. Anal. Chem. 29:1702–1706.

[18] Greer AL (1982) Crystallization kinetics of $Fe_{80}B_{20}$ glass. Acta Metall. 30:171–192.

[19] Henderson D W (1979) Thermal analysis of non-isothermal crystallization kinetics in glass forming liquids. J. Non-Cryst. Solids 30:301–315.

[20] Galwey AK, Brown ME (1998) Kinetic background to thermal analysis and calorimetry. Handbook of thermal analysis and calorimetry: principles and practice. Brown ME, editor. Elsevier Science B.V. pp. 147-224.

[21] Christian JW (1975) The Theory of Transformations in Metals and Alloys. Pergamon, Oxford p. 542.

[22] Avrami M (1939) Kinetics of phase change I. J. Chem. Phys. 7: 1103-1112.

[23] Avrami M (1940) Kinetics of phase change II. J. Chem. Phys. 8: 212-224.

[24] Avrami M(1941) Kinetics of phase change III. J. Chem. Phys. 9: 177-184.

[25] Kolmogorov AN (1937) Statistical theory of crystallization of metals. Bull. Acad. Sci. USSR, Phys. Sci.1:355-359.

[26] Moumeni H, Alleg S, Greneche JM (2006), Formation of ball-milled Fe-Mo nanostructured powders. J. Alloys Compd. 419: 140-144.

[27] Souilah S, Alleg S, Djebbari C, Suñol JJ (2012) Magnetic and microstructural properties of the mechanically alloyed $Fe_{57}Co_{21}Nb_7B_{15}$ powder mixture. Mat. Chem. Phys. 132: 766-772.

[28] Alleg S, Hamouda A, Azzaza S, Suñol JJ, Greneche JM (2010) Solid state amorphization transformation in the mechanically alloyed $Fe_{27.9}Nb_{2.2}B_{69.9}$ powders. Mat. Chem. Phys. 122: 35-40.
[29] Alleg S, Bensalem R (2011) Nanostructured Fe-based Mixtures Prepared by Mechanical Alloying. In: Jason M. Barker, editor, Powder Engineering, Technology and applications, Nova Science Publishers: pp. 81-124.
[30] Louidi S, Bentayeb FZ, Suñol JJ, Escoda L (2010) Formation study of the ball-milled $Cr_{20}Co_{80}$ alloy. J. Alloys Compd. 493: 110-115.
[31] Loudjani Nadia, Bensebaa Nadia, Alleg Safia, Djebbari Chaffia, Greneche Jean Marc (2011) Microstructure characterization of ball-milled $Ni_{50}Co_{50}$ alloy by Rietveld method. Phys. Status Solidi A 208:2124-2129.
[32] Calka A, Radlinski AP (1986) The effect of surface on the kinetics of crystallization of Pd-Si glassy metals. MRS Proceedings 80:195-201.
[33] Gibson MA, Delamore GW (1987) Crystallization kinetics of some iron-based metallic glasses. J. Mater. Sci. 22:4550-4557.
[34] Cao M G, Fritsch HU, Bergmann HW (1985). Thermochim. Acta 83:23.
[35] Lü L, Lai M (1998) Mechanical alloying. Kluwer Academic Publishers. 273 p.
[36] Ibrir M (2011) PhD Thesis. Badji Mokhtar Annaba University, Algeria.
[37] Moumeni H, Alleg S, Greneche JM (2005) Structural properties of $Fe_{50}Co_{50}$ nanostructured powder prepared by mechanical alloying. J. Alloys Compd. 386: 12-19.
[38] Moumeni Hayet, Nemamcha Abderrafik, Alleg Safia, Greneche Jean-Marc (2010) Stacking faults and structure analysis of ball-milled Fe-50%Co powders. Mat. Chem. Phys. 122:439-443.
[39] Brüning R, Samwer K, Kuhrt C, Schultz L (1992) The mixing of iron and cobalt during mechanical alloying. J. Appl. Phys. 72:2978-2983.
[40] Sorescu M, Grabias A (2002) Structural and magnetic properties of $Fe_{50}Co_{50}$ system. Intermetallics 10:317-321.
[41] Lutterotti L (2000) MAUD CPD Newsletter (IUCr) 24.
[42] Lutterotti L, Matthies S, Wenk HR (1999) MAUD: a friendly Java program for material analysis using diffraction. IUCr: Newsletter of the CPD, 21:14-15.
[43] Li S, Wang K, Sun L and Wang Z (1992) Simple model for the refinement of nanocrystalline grain size during ball milling. Scr. Metall. Mater. 27: 437-442
[44] Börner I, Eckert J (1997) Nanostructure formation and steady-state grain size of ball-milled iron powders. Mat. Sci. Eng. A226-228: 541-545.
[45] Fecht HJ (1994) Nanophase Materials. In:Hadjipanayis G C, Siegel R W, editors. 260:125-132
[46] Zhou GF, Bakker H (1994) Atomically disordered nanocrystalline Co_2Si by high-energy ball milling. *J. Phys.: Condens. Matter. 6:4043*–4052.
[47] McHenry ME, Gallagher K, Johnson F, Scott JH, Majetich SA (1996) Recent advances in the chemistry and physics of fullerenes and related materials. In: Kadish KM, Ruoff RS, editors. PV96-10, ECS Symposium Proceedings, Pennington, NJ, p. 703.

[48] Host J J, Teng M H, Elliot B R, Hwang J H, Mason T O, Johnson D L (1997) Graphite encapsulated nanocrystals produced using a low carbon:metal ratio. J. Mat. Res. 12: 1268-1273.

[49] Krill C E, Merzoug F, Krauss W and Birringer R (1997) Magnetic properties of nanocrystalline Gd and *W*/Gd. NanoStruct. Mater 9:455-460.

[50] Massalski T (1990) Binary alloy phase diagrams, Materials Park OH: ASM International.

[51] Turgut Z, Huang MQ, Gallagher K, McHenry ME (1997) Magnetic evidence for structural phase-transformations in Fe-Co alloy nanocrystals produced by a carbon arc. J. Appl. Phys. 81: 4039-4041.

[52] Persiano AIC, Rawlings RD (1991) Effect of niobium additions on the structure and magnetic properties of equiatomic iron cobalt alloys. J. Mat. Sci. 26: 4026-4632.

[53] Bensalem R, Younes A, Alleg S, Souilah S, Azzaza S, Suñol JJ, Greneche JM (2011) Solid state amorphisation of mechanically alloyed Fe-Co-Nb-B alloys. Int. J. Nanoparticles 4: 45-52.

[54] Alleg S, Souilah S, Bensalem R, Younes A, Azzaza S, Suñol JJ(2010) Structural characterization of the mechanically alloyed $Fe_{57}Co_{21}Nb_7B_{15}$ powders. Int. J. Nanoparticles 3: 246-256.

[55] Alleg S, Souilah S, Achour Y, Suñol JJ, Greneche JM (2012) Effect of the Nb content on the amorphization process of the mechanically alloyed Fe-Co-Nb-B powders. J. Alloys Compd. 536S:S394-S397.

[56] Blazquez JS, Conde A, Greneche JM (2002) Mössbauer study of FeCoNbBCu hitperm-alloys. Appl. Phys. Letters 81:1612-1614.

[57] Miglierini M, Greneche JM (1997) Mössbauer spectrometry of Fe(Cu)MB-type nanocrystalline alloys II: the topography of hyperfine interactions in Fe(Cu)ZrB alloys. J. Phys.: Condens. Matter 9:2321-2347.

[58] Suñol JJ, Güell JM, Bonastre J, Alleg S (2009) Structural study of nanocrystalline Fe-Co-Nb-B alloys prepared by mechanical alloying**.** J. Alloys Compd. 483: 604-607.

[59] Gercsi Zs, Mazaleyrat F, Kane SN, Varga LK (2004) Magnetic and structural study of $(Fe_{1-x}Co_x)_{62}Nb_8B_{30}$ bulk amorphous alloys. Mater. Sci. Eng. A 375–377: 1048-1052.

[60] Gloriant T, Suriňach S, Baró MD (2004) Stability and crystallization of Fe-Co-Nb-B amorphous alloys. J. Non-Crystal. Sol. 333: 320-326.

[61] Hernando A, Navarro I, Gorría P (1995) Iron exchange-field penetration into the amorphous interphases of nanocrystalline materials. Phys. Rev. B 51:3281-3284.

[62] Suzuki K, Cadogan JM, Sahajwalla V, Inoue A, Masumoto T (1996) $Fe_{91}Zr_7B_2$ soft magnetic alloy. J Appl. Phys. 79: 5149-5151.

[63] Liebermann HH, Marti J, Martis RJ, Wong CP (1989) The effect of microstructure on properties and behaviours of annealed $Fe_{78}B_{13}Si_9$ amorphous alloy ribbon. Metall. Trans. A 20:63-70.

[64] Alleg S, Rihia G, Bensalem R, Suñol JJ (2009) Structural evolution of the ball-milled $Ni_{70}P_{30}$ powders. Ann. Chim. Sci. Mat. 34:267-273.

[65] Blazquez JS, Conde CF, Conde A (2001) Crystallization process in $(FeCo)_{78}Nb_6(BCu)_{16}$ alloys. J. Non-Cryst. Solids 287:187-192.
[66] Souilah S (2012) PhD thesis. Badji Mokhtar Annaba University, Algeria.
[67] McHenry ME, Willard MA, Laughlin DE (1999), Amorphous and nanocrystalline materials for applications as soft magnets. Prog. Mat. Sci. 44:291-433.
[68] Bigot J, Lecaude N, Perron JC, Milan C, Ramiarinjaona C, Rialland JF (1994) Influence of annealing conditions on nanocrystallization and magnetic properties in $Fe_{73.5}Cu_1Nb_3Si_{13.5}B_9$ alloy. J. Magn. Magn. Mater. 133: 299-302.
[69] Shen SY, Hng HH, Oh JT (2004). Mater. Letter 58:2824.